

CHAPTER 98

TURBIDITY - SEDIMENTATION IN CLOSED-END CHANNELS

Chung-Po Lin¹, Jonathan W. Lott² and Ashish J. Mehta³

ABSTRACT: In order to investigate the mechanism by which turbidity currents cause sedimentation in closed-end channels such as pier slips or residential canals, a laboratory investigation using fine-grained sediments was carried out. Two similar flume systems were used, each consisting of a main channel carrying sediment-laden flow and an orthogonally placed closed-end channel with a gate at the entrance. Characteristics of the turbidity current and sediment deposition in the closed-end channel were investigated following gate opening. Behavioral similarities between turbidity current and non-settling gravity currents were observed. Several properties, e.g. suspension concentration, showed exponential-type decay with distance. The ratio of sediment settling velocity to the densimetric velocity was found to be a useful parameter for comparing different test results. A relationship for estimating the sediment influx through the entrance is presented.

INTRODUCTION

Sedimentation problems in closed-end channels such as pier slips, tidal docks and residential canals have been reported extensively (Lin, 1987). In a detailed investigation carried out in pier slips at the Mare Island Naval Shipyard, San Francisco Bay area, Jenkins et al. (1982) showed in quantitative terms that the rate of sedimentation in the slips was measurably higher than that in the main channel to which the slips were connected. In general, mass transport associated with the tidal prism, wind-driven circulation and density-induced currents are mechanisms by which sediment enters the slip. Turbidity current is essentially driven by the difference in density between the sediment-laden outside waters and the relatively quiescent and sediment-free waters in the slip. The contribution to the total rate of sedimentation from this mechanism varies with the physical conditions; where tides are weak or when the sediment concentration outside is high, turbidity current becomes important as the source of sediment in the slip.

¹Ph.D. Candidate, Coastal and Oceanographic Engineering Department, University of Florida, Gainesville, FL 32611.

²Research Engineer, Laboratoire National d'Hydraulique, Electricité de France, Chatou, France.

³Associate Professor, Coastal and Oceanographic Engineering Department, University of Florida, Gainesville, FL 32611.

In the presently described laboratory study, only fine-grained sediments were used. The transport of such sediments, particularly where the tides are weak, as in much of Florida, is predominantly episodically controlled. There, fair weather suspended sediment concentrations are typically quite low, on the order of 5-20 mg/L. Therefore the major contribution to slip sedimentation occurs mainly during storms, when concentrations increase by one or two orders of magnitude. Flume experiments were therefore designed with this characteristic of sediment transport in mind. Two conceptually similar flume systems were used, one at the Waterways Experiment Station (WES) of the U.S. Army Corps of Engineers, Vicksburg, Mississippi, and the other at the University of Florida's Coastal Engineering Laboratory (COEL).

A closed-end channel of length L and width B , orthogonally connected to the main channel, is shown in Figs. 1a,b. A turbidity front of instantaneous length x_f measured from the entrance ($x=0$) occurs. The mean depth of water is H above the horizontal bottom ($z=0$). The sediment-laden main channel flow is fully turbulent and vertically well-mixed. The fluid density there is $\rho_w + \Delta\rho_0$, where ρ_w is the clear water density and $\Delta\rho_0$ is the density increment due to suspended sediment. Immediately inside the entrance a gyre zone occurs in which circulation is driven by lateral flow shear at the entrance. The vertically mixed flow is weakly turbulent there, and the distance of influence of the gyre is limited, being of the same order as channel width B . Almost immediately inside the entrance, deposition of sediment commences and the suspension density is lower than that in the main channel. The density difference, $\Delta\rho_1$, is therefore characteristically lower than $\Delta\rho_0$. It was found that for most of the front-related phenomena observed, $\Delta\rho_1$ was better representative of the driving force than $\Delta\rho_0$. Beyond the gyre the flow is predominantly viscous and stratified, with a clearly identifiable interface ($z=n$). Three characteristic features of the forward portion of the front are the nose ($z=h_1$), head (h_2) and neck (h_3).

Initially the gate was closed with equal water levels on both sides, but without sediment in the closed-end channel. The objective was to investigate both the behavior of the front and the characteristics of sediment deposition. Opening the gate to allow the turbidity current to move in is, in a sense, analogous to the generation of a relatively high concentration front during a storm, over very low concentration ambient conditions representing fair weather. In examining the physical phenomena, the focus was on understanding the basic transport mechanisms, without explicit consideration for prototype to model scaling. For the sake of reference, however, it may be noted that, given typical prototype pier slips or residential canals, the selected flume dimensions (noted later) could be considered to represent a prototype to model ratio on the order of 1:20 to 1:40.

A characteristic feature of the turbidity front is that given a sufficiently long channel, front motion generally slows down, and is ultimately arrested at a distance where the finest particles in suspension (at the entrance) settle out. The fluid density decreases up to the nose, where it almost equals that of clear water. A steady state exists, and there is an overall balance of forces involving the

total density difference, water level set up in the channel and bottom friction. However, due to local force imbalance at different elevations above the bottom, sediment-laden water continues to enter through the lower half of the water column at the entrance, while an equal volume per unit time of almost sediment-free water leaves from the upper half.

METHODOLOGY

The three significant aspects of the phenomenon examined were: 1) the transient behavior of the propagating front after gate opening, 2) characteristics of the stationary front at steady state, and 3) rate of sedimentation. The scope of this paper permits only a brief presentation; details have been provided elsewhere (Lin and Mehta, 1986; Lott, 1986; Lin, 1987). In order to facilitate the investigation, three approaches were selected: 1) dimensional analysis for organizing the presentation of data, 2) numerical modeling to examine the transient and stationary front behaviors, and 3) simple analytic approaches to elucidate the stationary front behavior. Salient aspects are summarized below.

Dimensional Analysis

Dimensionless groups were developed for treating data for a number of different characteristics for the propagating as well as stationary fronts (Lin, 1987). One example will illustrate the point. The front speed, u_f , can be expressed as

$$\frac{u_f}{u_\Delta} = f \left(\frac{x}{H}, \frac{B}{H}, \frac{u_\Delta H}{\nu}, \frac{w_s}{u_\Delta} \right) \quad (1)$$

where ν is the kinematic viscosity of the fluid, and w_s is the sediment settling velocity. Furthermore, $u_\Delta = (g H \Delta \rho_1 / \rho_w)^{1/2}$, where g is acceleration due gravity, is recognized as the densimetric velocity. Equation 1 indicates that the dimensionless front speed should depend on the front position, x/H , channel aspect ratio, B/H , densimetric Reynolds number, $Re_\Delta = u_\Delta H / \nu$, and the relative settling velocity, w_s / u_Δ . This relationship is analogous to the result for the speed of the saline front advancing against river flow having a velocity, u_r . In that case, w_s is replaced by u_r (Keulegan, 1966).

Numerical Modeling

A two-dimensional (x, z) time-varying mathematical model was developed to predict the vertical and longitudinal suspension concentration fields, based upon a solution of the equation of flow momentum, continuity and sediment mass conservation. Unlike the case of salinity intrusion which depends, amongst other factors, on the imposed river flow velocity, flow circulation in the present case is due solely to the imposed density difference between the main channel and the closed-end channel. The equation of momentum is therefore inherently coupled with that of sediment mass conservation; hence these equations, together with that of continuity, must be solved simultaneously. This was done using a finite-difference scheme with

appropriate fluid mechanical and sediment-related surface, interface and bottom boundary conditions, as well as no-flow condition at the closed-end, and constant suspension concentration at the entrance.

The coefficients in the model requiring specification were: 1) longitudinal and vertical momentum and mass diffusion coefficients e_x , e_z and ϵ_x , ϵ_z , respectively, and Manning's n for bottom roughness. In addition, two deposition-related parameters, the settling velocity, w_s , and the critical stress for deposition, τ_{cd} were required. The latter is equal to the bed shear stress, τ_b , below which all initially suspended sediment (having uniform properties) eventually deposits, while for all τ_b greater than τ_{cd} no deposition occurs. Resuspension of the deposit did not occur, hence was not considered.

The model was tested for stability and convergence. Spatial increments $\Delta x = 0.5$ m and $\Delta z = 1$ cm, and time-step $\Delta t = 0.15$ sec were selected for all test simulations. Data from test COEL-4 were used for model calibration. Some model applications are presented here. By invoking the Reynolds analogy, $e_x = \epsilon_x$ and $e_z = \epsilon_z$ were assumed. Since the relatively low concentration flow was laminar everywhere except in the small gyre zone near the entrance, e_z was selected to be equal to the kinematic viscosity of water, 10^{-6} m²/sec. A value of 5×10^{-3} m²/sec was found to be adequate for e_x . These values of the coefficients, applicable to homogeneous flows, were modified in the model for representing stratified flows, through appropriate formulations involving the gradient Richardson number (Lin, 1987). Manning's n was selected to be 0.030, which was close to that obtained from the Moody diagram. The median (by weight) settling velocity, w_s , of fine-grained sediments varies with sediment concentration; hence its value in the channel is space and time-dependent. Thus, for example, within the concentration range of interest it was found that $w_s = 0.00001C^{0.78}$ for kaolinite, where w_s is in m/sec and concentration, C , is in mg/L. This empirical relationship was derived from an independent set of tests in a settling column (Lott, 1986). It was found practical to select a constant value of w_s for each test, for simulation purposes. The value, w_{s1} , representing the condition of the entrance, was chosen. An evaluation of kaolinite deposition data in the channel yielded a value of 0.13 N/m² for the critical stress, τ_{cd} .

Analytic Development

The occurrence of a stationary front permits, for that purpose, a simplification of the governing equations, which can be solved to yield approximate results. An advantage these offer over numerical results is that they demonstrate, via comparison with data, the significance of the more important forces in explaining observations related to the flow field and the suspension concentration field. Space does not permit presentation of the relevant derivations which are given elsewhere (Lin, 1987). Illustrative results are given here.

Flow Velocity: A stationary front occurs under a balance between gravity and viscous forces. The length of the stationary front can be assumed to be considerably greater than the still water depth, H . The water layer above the front is considered to be sediment-free; all the

sediment being confined to the lower layer, with a uniform concentration. Under these conditions, momentum diffusion can be shown to be much more important in the vertical than in the horizontal direction. The closed-end causes a water surface slope to be set up, with the hydrostatic head balancing the excess pressure due to the density gradient and the flow-induced bottom shear stress. In addition, inflow is balanced by outflow at every flow cross-section. Given the outflow velocity, u_s , at the surface, the following equations for the vertical profiles of the horizontal velocity, u , are obtained in the two layers:

$$\xi < \zeta < 1:$$

$$\frac{u}{u_s} = \frac{(1.5 - 0.375\xi)\zeta^2 - (3 - 0.75\xi)\zeta + 1}{-0.5 + 0.375\xi} \quad (2)$$

$$0 < \zeta < \xi:$$

$$\frac{u}{u_s} = \frac{(\zeta/\xi)^3 + (-3 + 1.5\xi^2 - 0.375\xi^3)(\zeta/\xi)^2 + (3 - 3\xi + 0.75\xi^2)(\zeta/\xi)}{-0.5 + 0.375\xi} \quad (3)$$

where $\zeta = z/H$ and $\xi = \eta/H$.

Concentration Below Interface: The longitudinal variation of the depth-mean concentration in the lower layer, C_b , can be examined by solving the steady state sediment mass transport equation. As a first order approximation only two terms need be considered: $u\partial C_b/\partial x$ and $w_s\partial C_b/\partial z$. Equating these terms amounts to balancing advective transport with gravitational settling. Experimental observations indicated an exponential-type decay for u and for w_s with distance (Lin, 1987). Therefore, $w_s = w_{s1} \exp(-\beta_1 x)$ and $u = u_1 \exp(-\beta_2 x)$ may be assumed, where subscript 1 for w_s and u refers to conditions at the entrance, and β_1 , β_2 are empirical coefficients. Without presenting further details, it suffices to state the following resultant relationship for \bar{C}_b :

$$\frac{\bar{C}_b}{\bar{C}_{b1}} = \exp \left[-\beta \left(\frac{w_{s1}}{u_1} \right) \left(\frac{x}{H} \right) \right] \quad (4)$$

where β depends on sediment properties. Investigations of lock exchange flows involving salinity-induced gravity currents suggest $\beta > 4$ (Lin, 1987).

Sediment Influx: The sediment influx rate at the entrance, $S = u_1 \bar{C}_1$, where \bar{C}_1 is the depth-mean concentration at the entrance. Experimental observations indicate that shortly after gate opening the flow velocity, u_1 , approaches a constant value (Gole *et al.*, 1973; Lin, 1987). Furthermore, both the initial front speed, u_{f1} , and u_1 depend on u_Δ . Thus, increasing u_Δ implies increasing u_{f1} and u_1 ; in fact observations indicate $u_{f1} \approx 0.5 u_\Delta$. Likewise, $u_1 = \alpha u_\Delta$ may be assumed, where α is a proportionality constant. Therefore $S = \alpha u_\Delta \bar{C}_1$. Expressing $\Delta\rho_1$ in terms of \bar{C}_1 , it can therefore be shown that

$$S = \alpha \left[\frac{gH}{\rho_w} \left(1 - \frac{1}{G_s} \right) \right]^{1/2} \bar{C}_1^{3/2} \quad (5)$$

where G_s is the specific gravity of the sediment. It is interesting to note that given the sediment-type and water depth, S is proportional uniquely to the $2/3$ power of sediment concentration at the entrance.

EXPERIMENTS

The dimensions of the closed-end channels at WES and COEL are given in Table 1. Also included are the imposed depth-mean concentration, C_o , in the main channel and the corresponding fluid density difference, $\Delta\rho_o$. Hydraulic arrangements were made to run each test for comparatively long durations (Lin, 1987). A total of 13 tests were carried out at WES and 14 at COEL. The longest test duration was 276 min in WES-13. Some difficulties were encountered in the WES tests in maintaining a constant water temperature during a test, owing to changes in the ambient air temperature. At COEL the flume was placed in a temperature-controlled environment. The test-mean temperature at WES ranged from 15.1 to 22.4°C, and at COEL from 18.9 to 26.7°C. In some tests, minor oscillations in otherwise steady flow speed and in suspension concentration in the main channel unavoidably resulted in data scatter.

Table 1. Summary of Experimental Conditions at WES and COEL

Flume	L (m)	B (m)	H (cm)	C_o (g/L)	$\Delta\rho_o \times 10^{-5}$ (g/cm ³)
WES	9.1	0.23	5.0-12.7	58-1878	3.4-114.7
COEL	14.7	0.10	8.0-10.6	250-3746	14.0-229.0

Seven fine-grained sediments together covering a wide range of physical and physico-chemical properties, were used; some cohesive and others nearly non-cohesive. The cohesive materials were flocculated, at fairly low salt concentrations in the fluid (Lin, 1987). Cohesive materials included kaolinite (median grain size 1 μm) and Cedar Key mud (2 μm). The others were flyash I (14 μm), flyash II (10 μm), flyash III (14 μm), Silica flour (7 μm) and Vicksburg loess (18 μm).

RESULTS

Front Characteristics

As in the case of the propagating front, for instance, of a salinity-induced gravity current, three distinct phases are found to occur during the movement of a turbidity front. These are the initial adjustment phase, the inertial phase and the viscous phase. These are

shown for COEL-5 (using kaolinite) in Fig. 2, in which the front position, x_f , is plotted against elapsed time after gate opening. The three phases are marked by lines of different slopes. During the first phase, of unit line slope, the front propagated at a constant speed, being motivated by the initial density gradient between the main and closed-end channels. During the second phase (line slope 2/3) inertia and gravity forces dominate, with the front speed, dx_f/dt , being proportional to $-1/3$ power of the elapsed time. For gravity currents, this $-1/3$ power dependence has been demonstrated both theoretically and experimentally (Rottman and Simpson, 1983). In the final phase, gravity and viscous forces entirely control front movement. The slope of 0.29 is slightly higher than $1/5$ observed in the case of a gravity current, partly because of the effects of thermal gradients during this test (Lin, 1987).

In several tests, the first phase was too short to be recorded. Furthermore, the point of transition from the second to the third phase was found to be strongly dependent upon the dimensionless settling velocity, w_{s1}/u_Δ . Thus, for example in COEL-5, characterized by $w_{s1}/u_\Delta = 0.0023$, transition occurred at about 400 min. after gate opening, while in COEL-8 (using flyash III), with $w_{s1}/u_\Delta = 0.0208$, transition occurred at about 50 min. Thus, in the latter case, the relatively large particles settled out rapidly, leaving behind a slow moving, very fine particle suspension influenced by viscous drag.

Dimensional analysis suggested that the dimensionless initial front speed u_{f1}/u_Δ , would possibly depend upon the densimetric Reynolds number, Re_Δ , and the channel aspect ratio, B/H . Data plotted in Fig. 3 from all WES and COEL tests show a fair degree of scatter, but no clear trend of dependence of u_{f1}/u_Δ on either Re_Δ or B/H . Part of the reason for the scatter is believed to be the influence of the entrance gyre zone on front propagation. The gyre length in the x-direction was in the range of 0.2-0.4 m in WES tests and 0.1-0.2 m in COEL tests. Therefore, the speed at $x=1$ m in WES tests and 0.75 m in COEL tests, rather than at $x=0$, was conveniently selected as the initial front speed. Notwithstanding the data scatter problem, the mean value of u_{f1}/u_Δ is observed to be 0.43, which is fairly close to the value 0.46 obtained by Keulegan (1957) for salinity currents. A value of 0.50 is obtained theoretically (Yih, 1965). Since the effect of sediment settling is much less significant than that of the density gradient at the beginning, the correspondence between gravity and turbidity currents in this respect is not surprising.

In Fig. 4, the ratio of front nose height to head height, h_1/h_2 is plotted against the local head Reynolds number, $Re_h = u_{fh}h_2/\nu$, for COEL tests (no data were collected at WES for this purpose). A trend of increasing h_1/h_2 with decreasing Re_h is evident. In other words, as might be expected, with increasing viscous drag relative to inertia, the nose becomes blunt, and nose height becomes greater relative to that of the head. In addition to COEL data, those on different types of gravity currents obtained from five other investigations have been included in Fig. 4 (Lin, 1987). The data of Lawson (1971) are shown by dashed lines indicating upper and lower bounds. These data, including those of Lawson's which are for gravity current in air, are observed to be entirely consistent with those from the present tests.

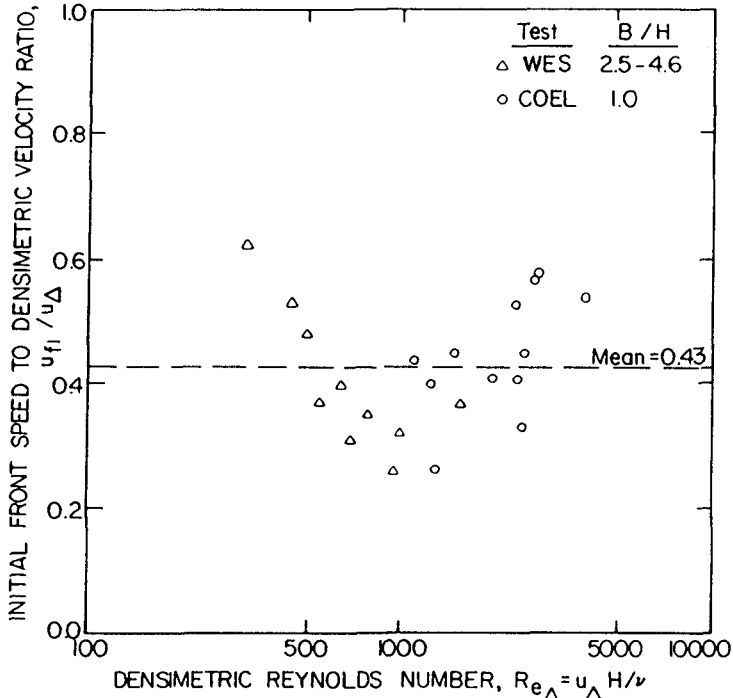


Fig. 3. Dimensionless Initial Front Speed against Densimetric Reynolds Number.

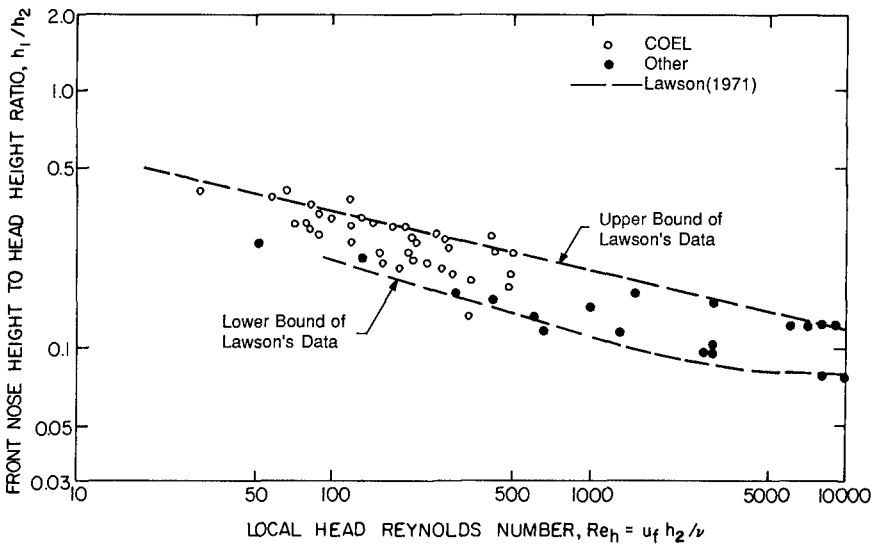


Fig. 4. Front Nose Height to Head Ratio against Local Head Reynolds Number.

Results presented by Lin (1987) indicate that the ratio of front head height to neck height, h_2/h_3 , independent of the local neck Reynolds number, $Re_n = u_f h_3 / \nu$, with a mean of 1.30. For salinity data at somewhat higher Reynolds numbers, Keulegan (1958) obtained a similar result with a mean of 2.08.

Velocity Profiles

For illustration, only results on the vertical velocity profiles at steady state, corresponding to a stationary front, are presented here. In Fig. 5, the dimensionless horizontal velocity, $u/|u_s|$ is plotted against the corresponding dimensionless elevation, $\zeta = z/H$. The data are for COEL-6 at $x=1.8$ m. Comparison has been made with numerical results as well as with analytically derived Eqs. 2 and 3. The numerical result is not affected by the boundary layer effects associated with the side walls of the channel. The data were obtained via a dye injection procedure such that the results were influenced both by the wall boundary and by lateral secondary currents. Limitations of the analytic solutions were noted previously. In spite of these evident differences, the agreement between measured data, numerical and analytic results may be considered to be acceptable. The numerical and analytic results satisfy the steady state continuity requirement of equal discharge both ways. Experimental data are inaccurate in this respect.

Concentration Profiles

In Fig. 6, suspension concentration at elevation $z=0.7$ cm at five horizontal locations in COEL-5 are plotted as a function of time. At each location this elevation was below the corresponding elevation of the front interface. At each location, the concentration rises from nil ahead of the front to an eventual steady state value. Numerical results compare reasonably well with the data.

In Fig. 7, vertical concentration profiles for COEL-5 are plotted at 67 and 90 min. after gate opening. Five horizontal locations have been included. Agreement between data and numerical results (at 130 min) appears to be acceptable. The total height of each profile corresponds to the thickness of the turbid lower layer at that position and time.

Both the exponential nature of concentration decay with distance and the influence of the dimensionless settling velocity, w_{s1}/u_Δ , on the concentration profile is apparent in Fig. 8, in which the concentration ratio, C_b/C_{b1} at steady state is plotted against x/H on semi-logarithmic coordinates. Data from seven tests using kaolinite have been included. The exponential nature of the profiles is apparent. Three lines represented by different values of w_{s1}/u_Δ have been shown. Line slope is observed to increase with increasing w_{s1}/u_Δ , as would be expected since, for a given u_Δ , increasing w_{s1} implies increasing rate of deposition of sediment from suspension. These w_{s1}/u_Δ values (indicated on the lines) were obtained by best fitting Eq. 4 to data using $\beta=7$. It can be shown that this value of β corresponds to the ratio $u_1/u_{f1} = 0.57$, which is close to the value, 0.70, obtained experimentally by Gole et al. (1973). These w_{s1}/u_Δ

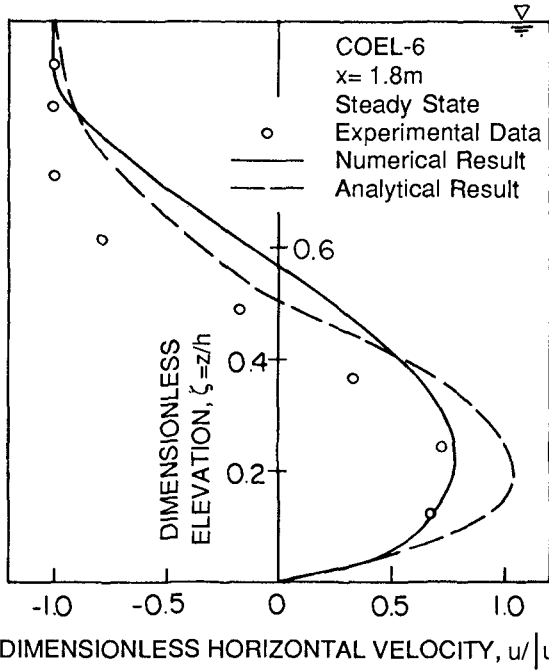


Fig. 5. Dimensionless Horizontal Velocity Profiles, Test COEL-6 at $x = 1.8\text{ m}$.

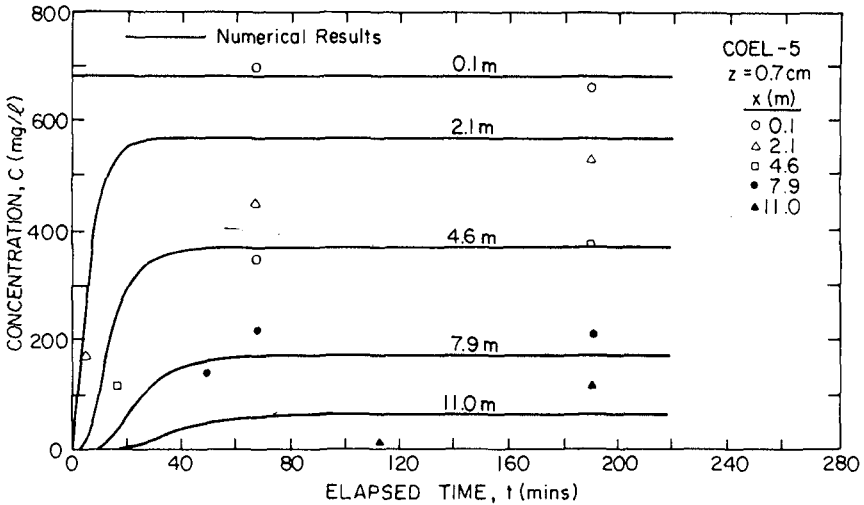


Fig. 6. Suspension Concentration at 0.7 cm Elevation for Five Locations as a Function of Elapsed Time after Gate Opening, Test COEL-5.

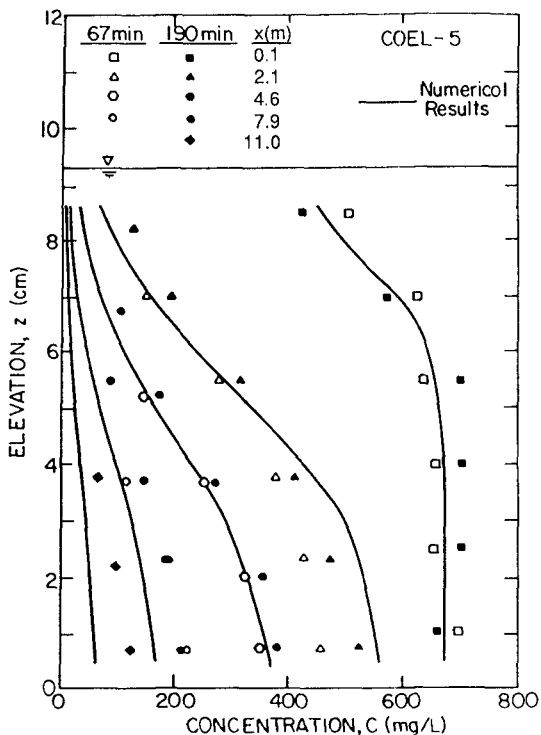


Fig. 7. Concentration Profiles at Steady State at Five Locations, COEL-5

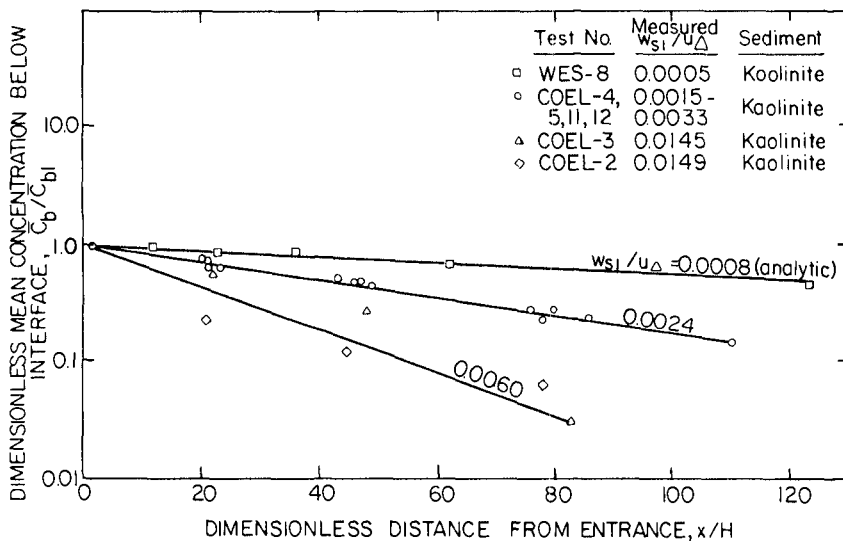


Fig. 8. Dimensionless Mean Conc. below Interface against Dist., Kaolinite

values differ from those based on measurement as given within the figure. The discrepancy increases with increasing w_{s1}/u_{Δ} , as a result of inherent limitation in applying Eq. 4 to data on sediment with a relatively large settling velocity. In such an event, for instance, the vertical concentration gradient becomes pronounced; hence the assumption of a uniform concentration, inherent in Eq. 4, is no longer reasonable.

Sediment Deposition and Influx

Sorting of sediment was characteristically observed in all tests in which relevant data were collected, with the grain size generally decreasing with distance from the entrance. Qualitatively, the same trend has been reported in prototype canals (Wanless, 1975). For nearly cohesionless sediment such as flyash, sorting measurably increased with increasing w_{s1}/u_{Δ} .

In Fig. 9, the rate of deposition, δ , is plotted against distance from the entrance for COEL-5. As would be expected, δ is observed to decrease rapidly with distance, once again suggesting an exponential decay. Agreement between measurement and numerical prediction is acceptable, except that there is a slight over-prediction.

Based upon the concept presented earlier, the rate of sediment influx, S , is plotted against entrance concentration, \bar{C}_1 in Fig. 10. A $3/2$ power dependence of S on \bar{C}_1 is clearly evident in accordance with Eq. 5. Note that S represents a mean value, which was calculated by dividing the total deposited sediment mass in the channel by the test duration and the area of the lower half of the flow cross-section at the entrance. Since the turbidity front moved in fairly slowly during most of test duration except at the very beginning, S can be practically considered to represent the sediment influx rate as would occur at steady state. The coefficient 0.015 was calculated by selecting mean values of $H = 8.8$ cm and $G_s = 2.55$, for the twelve selected tests. The value $\alpha = 0.35$ was empirically chosen, but this value can be shown to be consistent with the observations of Gole et al. (1973) that at steady state, the surface outflow velocity at the entrance is about 30% lower than the initial front speed (Lin, 1987).

CONCLUDING REMARKS

It is worthwhile noting in summary, that the turbidity current behaves generally in the same manner as a gravity current induced, for instance, by salinity, although there are evident differences, principally characterized by the ratio w_{s1}/u_{Δ} , a conveniently measurable parameter related to the turbidity current.

Although no attempt could be made in discussing model to prototype scaling problems because of evident reasons, it is noteworthy that by giving consideration to the basic fluid mechanical laws relating to the observed phenomena, a framework for future prototype investigation of a comprehensive nature is believed to have been established. Comparison may be made here between the present study and similar, very useful, previous investigations in laboratories on salinity-driven gravity currents.

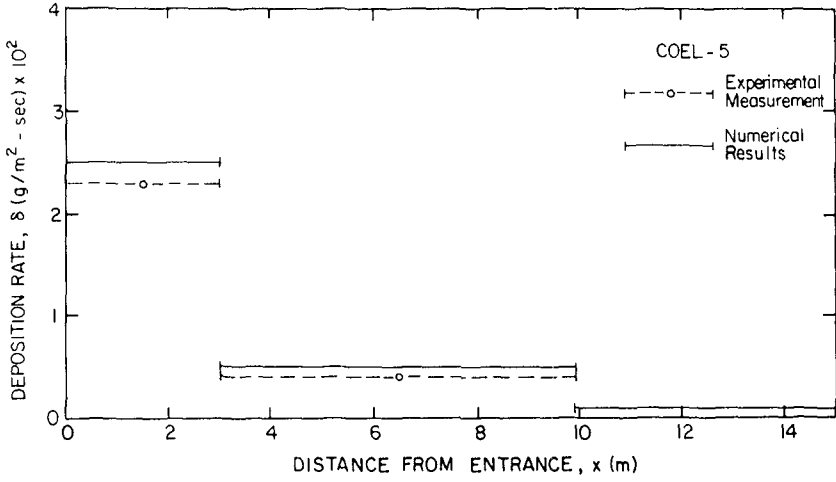


Fig. 9. Variation of Rate of Deposition with Distance, Test COEL-5.

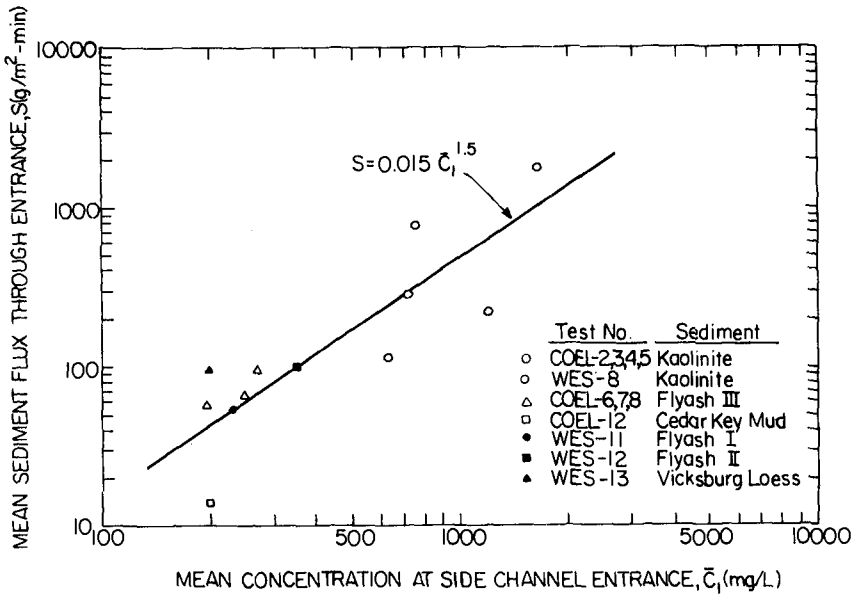


Fig. 10. Mean Sediment Flux as a Function of Depth-Mean Entrance Concentration.

From an engineering application viewpoint, Eq. 5 and its confirmation through Fig. 10 provide a simple means for computing the rate of sedimentation in closed-end channels. Its application to prototype canals seems highly promising, and deserves further consideration in that context.

ACKNOWLEDGEMENT

Support of the National Science Foundation (Grant No. CEE-84-01490), and the Hydraulics Laboratory of the Waterways Experiment Station, Vicksburg, Mississippi, is sincerely acknowledged.

REFERENCES

- Gole, C.V., Tarapore, Z.S., and Gadre, M.R., "Siltation in Tidal Docks due to Density Currents," Proceedings of the Fifteenth Congress of I.A.H.R., Vol. 1, Istanbul, Turkey, 1973, pp. 335-340.
- Jenkins, S.A., Inman, D.L., and Bailard, J.A., "Opening and Maintaining Tidal Lagoons and Estuaries," Proceedings of the Seventeenth Coastal Engineering Conference, ASCE, Vol. II, Sydney, Australia, 1980, pp. 1528-1547.
- Keulegan, G.H., "An Experimental Study of the Motion of Saline Water from Locks into Fresh Water Channels," Report No. 5168, National Bureau of Standards, Washington, DC, March, 1957.
- Keulegan, G.H., "The Motion of Saline Fronts in Still Water," Report No. 5831, National Bureau of Standards, Washington, DC, April, 1958.
- Keulegan, G.H., "The Mechanism of an Arrested Saline Wedge," Estuary and Coastline Hydrodynamics, A.T. Ippen Editor, Ch. 11, McGraw-Hill, New York, 1966, pp. 546-574.
- Lawson, T.J., "Haboob Structure at Khartoum," Weather, Vol. 26, 1971, pp. 105-112.
- Lin, C.P., "Turbidity Currents and Sedimentation in Closed-End Channels," Ph.D. Dissertation, University of Florida, Gainesville, 1987.
- Lin, C.P., and Mehta, A.J., "Sediment-driven Density Fronts in Closed End Canals," Physics of Shallow Estuaries and Bays, Lecture Notes on Coastal and Estuarine Studies Series, Vol. 16, J. van de Kreeke Editor, Springer-Verlag, Berlin, 1986, pp. 259-276.
- Lott, J.W., "Laboratory Study on the Behavior of Turbidity Current in a Closed-End Channel," M.S. Thesis, University of Florida, Gainesville, 1986.
- Rottman, J.W., and Simpson, J.E., "Gravity Currents Produced by Instantaneous Releases of a Heavy Fluid in a Rectangular Channel," Journal of Fluid Mechanics, Vol. 135, 1983, pp. 95-110.
- Wanless, H.R., "Sedimentation in Canals," Report, Division of Marine Geology and Geophysics, Rosenstiel School of Marine and Atmospheric Science, University of Miami, Miami, Florida, 1975.
- Yih, C.S., Dynamics of Nonhomogeneous Fluids, Macmillan, New York, 1965.